

High-precision baryon number cumulants from lattice QCD in a finite box: cumulant ratios, Lee-Yang zeros and critical endpoint predictions

Alexander Adam,¹ Szabolcs Borsányi,¹ Zoltán Fodor,^{2,1,3,4} Jana N. Guenther,¹

Piyush Kumar,¹ Paolo Parotto,⁵ Attila Pásztor,³ and Chik Him Wong¹

¹*Department of Physics, Wuppertal University, Gausstr. 20, D-42119, Wuppertal, Germany*

²*Pennsylvania State University, Department of Physics, State College, PA 16801, USA*

³*Institute for Theoretical Physics, ELTE Eötvös Loránd University,*

Pázmány P. sétány 1/A, H-1117 Budapest, Hungary

⁴*Jülich Supercomputing Centre, Forschungszentrum Jülich, D-52425 Jülich, Germany*

⁵*Dipartimento di Fisica, Università di Torino and INFN Torino, Via P. Giuria 1, I-10125 Torino, Italy*

(Dated: July 18, 2025)

We have performed high-statistics lattice simulations using 4HEX improved staggered fermions on $16^3 \times 8$ lattices. We calculated the Taylor expansion coefficients of the pressure with respect to the baryochemical potential to the tenth order at zero, and fourth order at purely imaginary chemical potentials. We used this data to construct rational function approximations of the free energy. We use a rational ansatz that explicitly satisfies the charge conjugation symmetry and the Roberge-Weiss periodicity, which are exact properties of the QCD free energy. We use this ansatz to estimate the position of Lee-Yang zeros in the complex chemical potential plane. The temperature dependence of the imaginary part of the Lee-Yang zeros is then fitted with ansätze motivated by the universal behavior of the free energy near a 3D Ising critical point. In principle, this allows one to estimate the temperature of the critical endpoint. We consider several sources of systematic errors. On this single lattice spacing we find that with 84% probability, the chiral critical endpoint is either below 103 MeV temperature or it does not exist. We also identify some caveats of the method, which do not disappear even with the extremely high statistics of this present study. We discuss to what extent these can be eliminated by future high statistics lattice analyses.

I. INTRODUCTION

A major goal of heavy-ion physics research is the exploration of the phase diagram of strongly interacting matter in the temperature(T)-baryon density (or baryochemical potential μ_B) plane. Although it is well established that the transition between quarks and hadrons at $\mu_B = 0$ is a smooth crossover [1], our knowledge of the phase diagram at $\mu_B > 0$ is limited.

First-principles lattice QCD calculations are hampered by the sign problem, severely limiting the region in μ_B where results are available. Some well-established quantities determined with a lattice QCD approach include the curvature of the phase diagram at $\mu_B = 0$ [2–4] and the derivatives of the pressure with respect to the chemical potentials [5–7].

Higher chemical potentials are explored with chiral effective model calculations [8, 9], truncated Dyson-Schwinger equations [10, 11] and holography-based modeling [12]. These approaches tend to predict a critical endpoint where the crossover line becomes a line first-order transition, at higher values of the baryochemical potential.

Recently, the lattice QCD community has developed extrapolation schemes that can reach higher values of the chemical potentials and thus shed some light on the position of the coveted critical endpoint. These extrapolations employ lattice QCD data collected either at zero or purely imaginary chemical potentials. A general property of these methods is that they are based on ansätze for the free energy that are not polynomials in the chemical

potential. Such a non-polynomial structure is necessary to capture the onset of a true phase transition, which leads to non-analytic behavior in the free energy.

Two related approaches include the T' expansion [13–17] and the extrapolation of contours of constant entropy [18–20]. The current state-of-the-art using this approach is a 2σ lower bound on the position of the critical endpoint at $\mu_B \approx 450\text{MeV}$.

In this manuscript we study Lee-Yang zeros, which offer a different approach to the study of the phase diagram [5, 21–26], by means of a two-step extrapolation (see Ref. [27] for a detailed explanation). In the first step, one extrapolates to the complex μ_B plane at a fixed value of the temperature T . The goal of this first step is to estimate the position of Lee-Yang zeros. These are zeros of the partition function, logarithmic branch points of the free energy and poles of the baryon number and baryon number susceptibility. At temperatures where the transition at $\mu_B > 0$ is a crossover, the position of these zeros has a non-vanishing imaginary part. In the second step of the approach, one then attempts to extrapolate the value of this imaginary part to lower temperatures, to estimate where it becomes zero. This provides an estimate of the critical endpoint (CEP) position. Recent CEP estimates using this approach include Refs. [25, 26].

Both steps of this two-step approach can potentially suffer from large systematic uncertainties. The main goal of this manuscript is to estimate the uncertainties of both of these steps, and to see how they propagate to the final predictions on the critical endpoint position, thus testing the reliability of the approach. We will show that the

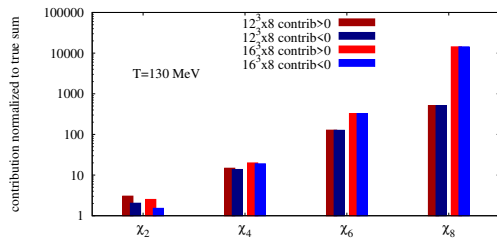


FIG. 1. Cancellations between positive and negative terms for the Taylor coefficients χ_n for up to the eighth order at $T = 130$ MeV. Positive contributions are shown in red, while negative contributions are shown in blue. A smaller volume ($12^3 \times 8$) is also shown, to illustrate the volume dependence of the cancellations.

systematics, especially of the second extrapolation, are quite substantial. This means that instead of a sharp prediction on the CEP position, the extrapolations only give an upper bound on the temperature of the critical endpoint. We conduct this study in a setting where we have very accurate input data: in a finite volume and at finite lattice spacing. This means that inevitably our results are subject to volume and cut-off effects. We cannot yet provide an estimate of the systematic errors related to these effects, and leave that for future work.

The structure of this manuscript is as follows. We explain the lattice setup in the next section. In section 3 we present our results for the baryon chemical potential derivatives we will use in the subsequent analysis of Lee-Yang zeros. This section also includes simple - Taylor expansion based - estimates of the phenomenologically relevant fourth to second and third to first cumulant ratios at non-zero μ_B . In section 4 we present our analysis of the Lee-Yang zeros based on a rational function approximation and the subsequent extrapolation of the CEP position. We will emphasize the source of different systematic errors and finally show a posterior distribution for the estimated CEP position. Our results include a systematic error estimate of the two different extrapolation steps. However, we note that, at present, potentially one of the most important sources of systematic uncertainties – namely the temperature range used for the extrapolation to the critical point – cannot be estimated, due to the limited range in the available lattice data. This is a feature that our study shares with other studies available in the literature.

II. BARYON NUMBER FLUCTUATIONS FROM LATTICE QCD

A. Lattice observables and simulation details

We use a fixed lattice size $16^3 \times 8$, meaning that our physical volume is fixed in temperature units to $LT = 2$. We use ensembles with 4HEX staggered fermions as in our recent works [6] and [28], but the statistics was in-

creased considerably to around 2 million configurations per temperature. Furthermore, we also simulated lattices at eight imaginary values of the chemical potential, with a statistics of around 100,000 configurations per temperature and chemical potential (see statistics in Table I in Appendix C).

For this partly conceptual study, we set $\mu_S = 0$, as opposed to the more physical setting of strangeness neutrality $n_S = 0$. (This more physical setting was adopted in our recent work on contours of constant entropy in Ref. [19].)

Similarly to our previous work in Refs. [6, 29–33] we used the reduced matrix formalism [34] to obtain the configuration-specific expansion coefficients to arbitrary order. This, together with our high statistics ensembles, allowed us to calculate Taylor coefficients at $\mu_B = 0$ to an unprecedented order $\mathcal{O}(\mu_B^{10})$. At purely imaginary chemical potentials we calculated Taylor coefficients up to order $\mathcal{O}(\mu_B^4)$. Note that at nonzero imaginary chemical potential the odd derivatives are also nonvanishing, in contrast to $\mu_B = 0$ where only even derivatives appear in the Taylor expansion. Up to the sixth order in the Taylor expansion we observed moderate cut-off dependence in this discretization scheme [6].

Our study of the Lee-Yang zeros is made possible by the impressive dataset on baryon number fluctuations that the generated statistics has allowed us to obtain. Thus, we start with the fluctuation results.

In Fig. 2 we show the μ_B -derivatives of the pressure

$$\chi_n = \left(\frac{\partial^n (p/T^4)}{\partial (\mu_B/T)^n} \right)_{\mu_B=0}, \quad (1)$$

as functions of temperature on our ensembles. Due to our fixed volume setup, we can calculate the sixth and eighth derivatives to unprecedented precision. In addition, for the first time in the literature, we provide a calculation of the tenth order coefficient as well.

There are several strategies for the computation of high order baryon fluctuations. The standard procedure involves the use of random sources to compute the configuration-specific coefficients. These enter in connected and disconnected diagrams [35]. We, however, follow Ref. [6] and use the exact representation of the quark determinant as function of μ , since for the given lattice size this approach is more economic, and potentially more precise. Even if only a single quark chemical potential is considered, the number of terms in the expression for χ_2, \dots, χ_{10} is 2, 8, 25, 79, 230, respectively. Although we do not face a complex action problem while we compute the χ_n coefficients, a remnant cancellation problem appears through the cancellation between these terms, contributing to the same χ_n . We illustrate the severity of the problem in Fig. 1. For two lattice volumes we show the magnitude of the sum of all positive and all negative terms, respectively. These are constructed in such a way, that the actual signal – namely the difference between positive and negative contributions – equals 1. With each successive order the severity grows with a

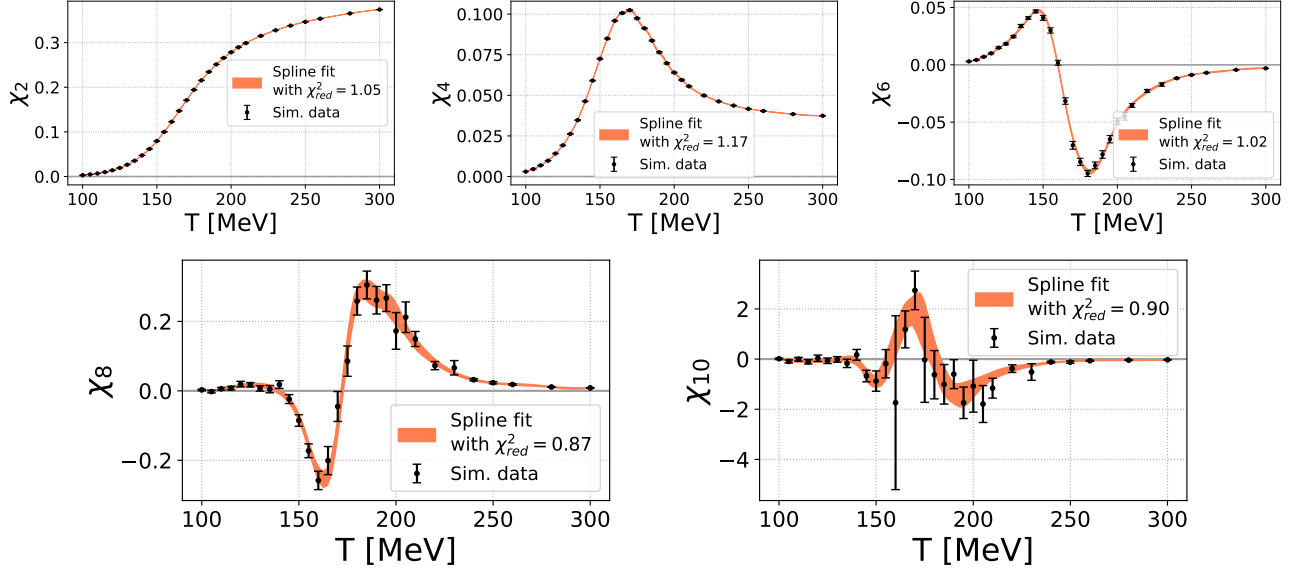


FIG. 2. Derivatives of the pressure with respect to the baryo-chemical potential at $\mu_B = 0$ as functions of the temperature T on our $16^3 \times 8$ 4HEX ensembles, together with a spline interpolation of the data points.

volume-dependent factor. This plot explains why we refrain at present from the use of larger volumes, and why more standard volumes, such as $32^3 \times 8$, are hopelessly unfeasible.

We emphasize that for the data in Fig. 2 we did not include input from imaginary- μ ensembles, thus the results do not rely on any sort of analytical assumption.[36]

B. Fluctuations at non-zero chemical potential

Given the data in Fig. 2, one can perform simple Taylor extrapolations of several different fluctuation observables to non-zero μ_B . For even derivatives we have:

$$\chi_{2n}^B(T, \mu_B) = \left(\frac{\partial^{2n}(p/T^4)}{\partial(\mu_B/T)^{2n}} \right)_{\mu_B} \quad (2)$$

$$= \chi_{2n} + \chi_{2n+2} \frac{\hat{\mu}_B^2}{2!} + \chi_{2n+4} \frac{\hat{\mu}_B^4}{4!} + \dots, \quad (3)$$

while for odd derivatives, we have:

$$\chi_{2n+1}^B(T, \mu_B) = \left(\frac{\partial^{2n+1}(p/T^4)}{\partial(\mu_B/T)^{2n+1}} \right)_{\mu_B} \quad (4)$$

$$= \chi_{2n+1} + \chi_{2n+3} \frac{\hat{\mu}_B}{1!} + \chi_{2n+5} \frac{\hat{\mu}_B^3}{3!} + \dots, \quad (5)$$

where we have introduced the shorthand notation $\hat{\mu}_B = \frac{\mu_B}{T}$. Note that we adopt the notation where

$$\chi_n(T) \equiv \chi_n^B(T, \mu_B = 0).$$

We show $\chi_2^B(T, \mu_B)$ from a Taylor expansion up to order χ_{10} in Fig. 3. At chemical potentials above 500 MeV

the estimate shows the characteristic sign structure of χ_{10} from Fig. 2, indicating that at such high chemical potentials, the highest Taylor coefficient dominates the estimate. This means that without a further order in the expansion, the correctness of this estimate at such high chemical potentials cannot be tested.

Ratios of fluctuations have also been studied in the literature. In particular χ_4^B/χ_2^B is interesting, as it is expected to show a non-monotonic behavior near the CEP, which can potentially be seen quite far away from the CEP position itself [37–39]. Another interesting ratio is χ_3^B/χ_1^B , as it should change sign near the crossover in the vicinity of the CEP.

Although the Taylor expansion coefficients of ratios such as χ_3^B/χ_1^B and χ_4^B/χ_2^B have been calculated in the literature before, this approach is not suitable to reach high chemical potentials. This is because the radius of convergence of the Taylor expansion of the ratio χ_4^B/χ_2^B in the variable μ_B/T is close to $\pi/2$ at low temperatures. This radius of convergence is unrelated to the critical endpoint, and is due to a zero of χ_2^B at purely imaginary chemical potentials. This is explained in some details in Appendix A. Thus, this particular radius of convergence has nothing to do with the CEP, but it makes a direct Taylor expansion of the ratio χ_4^B/χ_2^B less useful.

A safer approach is, thus, to Taylor expand the numerator and denominator separately:

$$\frac{\chi_4^B(T, \mu_B)}{\chi_2^B(T, \mu_B)} \approx \frac{\chi_4 + \chi_6 \frac{\hat{\mu}_B^2}{2} + \chi_8 \frac{\hat{\mu}_B^4}{4!} + \chi_{10} \frac{\hat{\mu}_B^6}{6!}}{\chi_2 + \chi_4 \frac{\hat{\mu}_B^2}{2} + \chi_6 \frac{\hat{\mu}_B^4}{4!} + \chi_8 \frac{\hat{\mu}_B^6}{6!} + \chi_{10} \frac{\hat{\mu}_B^8}{8!}} \quad (6)$$

and similarly for χ_3^B/χ_1^B . The results of this approximation are shown in Fig. 4. In both Figures, we see a similar structure as in χ_2^B itself: at large chemical potentials,

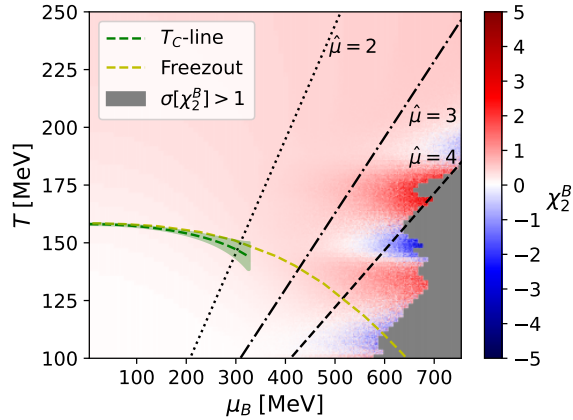


FIG. 3. $\chi_2^B(T, \mu_B)$ from a Taylor expansion to order χ_{10} , using the spline Taylor expansion coefficients from Fig. 2. We also show the crossover line from Ref. [4] and the chemical freezeout line from Ref. [40–43]. We added a noise to the color map to indicate the standard deviation of the observable. Additionally, the region where the magnitude of the absolute error exceeds 1 is shown in gray.

the highest order of expansion dominates. At this level of truncation the ratio χ_4^B/χ_2^B does show non-monotonic behavior, though the χ_3^B/χ_1^B ratio does not change sign near the transition and freeze-out lines. Thus, the picture is not completely consistent with the expected signatures of chiral criticality. Rather, the source of the non monotonic behavior of χ_4^B/χ_2^B is more likely to be the truncation of the Taylor series. We are directly facing the limitations of what is possible for our current dataset with Taylor extrapolation.

In order to have a more quantitative look at the phase diagram, we now turn to the discussion of Lee-Yang zeros.

III. LEE-YANG ZEROS FROM RATIONAL FUNCTION APPROXIMATIONS

A. Lee-Yang zeros

Lee-Yang zeros are zeros of the partition function in the complex chemical potential plane. For the case of a first-order phase transition they approach the real line at an infinite volume as $\text{Im } \mu_B \sim V^{-1}$, where V is the physical volume. In contrast, for a second order phase transition the zeros approach the real axis as $\text{Im } \mu_B \sim V^{-\frac{\gamma/\nu+D}{2D}}$, where γ and ν are the usual critical exponents and D is the dimensionality of space [44]. For 3D Ising critical exponents this corresponds to $\text{Im } \mu_B \sim V^{-0.83}$. In both the first and second order cases, an infinite number of zeros accumulates near the real line, leading to the singularity (phase transition) in the thermodynamic limit. For a crossover, there is no general formula for the volume scaling of the Lee-Yang zero positions, except for

the case when the crossover is in the immediate vicinity of a critical point. In this case, the finite volume scaling is of the form [44] $\text{Im } \mu_B \sim A + BV^{-\frac{1}{1+\sigma}}$, where σ is the so-called edge exponent. Its most common value [45, 46] is $\sigma \approx 0.076$, leading to the behavior:

$$\text{Im } \mu_B \sim A + BV^{-0.93}, \quad (7)$$

where A and B are non-universal amplitudes. Since we only have one volume in our study, we are going to assume that the second term is negligible $A \gg BV^{-0.93}$. The temperature dependence of A is given by the analytic continuation of the Kadanoff scaling ansatz to be:

$$\text{Im } \mu_B \sim A \sim |T - T_{CEP}|^{\beta\delta}, \quad (8)$$

where for the 3D Ising universality class the product of critical exponents $\beta\delta \approx 1.56$. By knowing $\text{Im } \mu_B$ for several temperatures above the temperature of the critical endpoint, Eq. (8) can be used to fit the temperature of the critical endpoint T_{CEP} . This basic approach, also used in Refs. [25, 26], is the one we pursue here.

In order to calculate such an estimate of T_{CEP} , one first needs to estimate the Lee-Yang zero positions at several fixed values of the temperature T . How this is achieved is discussed in the next subsection.

Here, we note that Eq. (8) is only valid in the close vicinity of the CEP. However, extracting the position of the Lee-Yang zeros at temperatures well below the crossover has so far proven to be prohibitively difficult. Thus, current extrapolations only use data in the vicinity of the crossover temperature (just below 160 MeV). This means that one is likely using data with sizable corrections to the scaling ansatz of Eq. (8). We will come back to this issue later, when we discuss the systematic errors on the CEP estimate.

B. Rational approximations and the choice of an expansion variable

To look for the Lee-Yang zeros, one needs a functional form for the baryon number susceptibilities that allows for the existence of poles. The simplest option is a rational function: the ratio of polynomials.

The direct lattice data from the simulations consist of Taylor expansion coefficients in μ_B^2 (see Fig. 2) at $\mu_B = 0$ (or in μ_B at non-zero imaginary μ_B). Only even terms appear in the Taylor expansion because of charge conjugation symmetry. Converting this Taylor series to a rational approximation leads to an ansatz of the form:

$$F(T, \mu_B) = \frac{p_0 + p_1 \hat{\mu}_B^2 + \dots + p_m \hat{\mu}_B^{2m}}{1 + q_1 \hat{\mu}_B^2 + \dots + q_n \hat{\mu}_B^{2n}}, \quad (9)$$

where F is some physical quantity of interest, such as χ_2^B . Such an ansatz was used in Ref. [26], where odd terms in μ_B were also allowed.

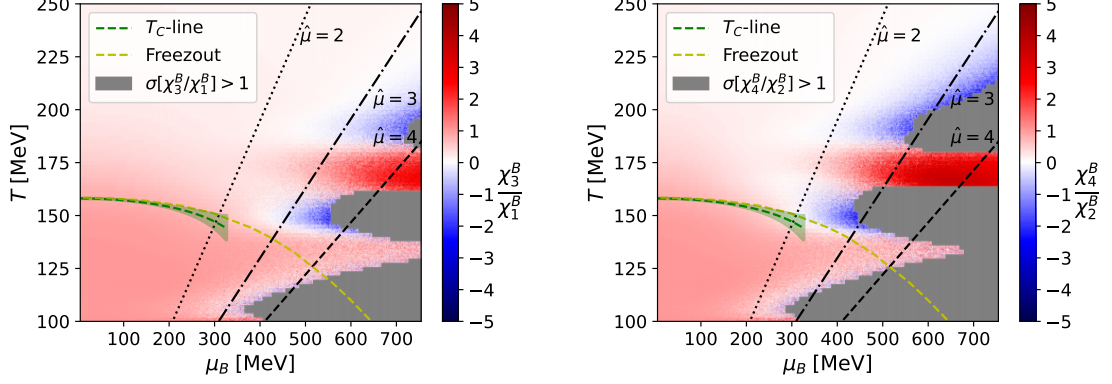


FIG. 4. $\chi_3^B(T, \mu_B)/\chi_1^B(T, \mu_B)$ (left) and $\chi_4^B(T, \mu_B)/\chi_2^B(T, \mu_B)$ (right) estimated using Eq. (6) and the splined Taylor expansion coefficients from Fig. 2. We added a noise to the color map to indicate the standard deviation of the observable. Additionally, the region where the magnitude of the absolute error exceeds 1 is shown in gray.

In general, one can use the chain rule to convert these expansion coefficients to expansion coefficients in different variables. The variable we will consider in this work is

$$x = \cosh(\hat{\mu}_B) - 1 = \frac{1}{2}\hat{\mu}_B^2 + \mathcal{O}(\hat{\mu}_B^4). \quad (10)$$

An expansion in this variable has two benefits. First, in the hadronic phase (below the crossover temperature) we expect this expansion to converge faster than a Taylor expansion: in the Boltzmann approximation of the ideal hadron resonance gas model, only the leading order term is non-zero. While this first term expresses the baryon density, the next order is responsible for the repulsive baryon interactions, and is suppressed by several orders in magnitude [47–49]. Another way to phrase this is: in this expansion variable, the leading order term is dominated by single baryons, while the next-to-leading order term is only non-zero in case of genuine two-baryon correlations. The second advantage of this variable is that it makes manifest use of the Roberge-Weiss symmetry: the periodicity of the QCD free energy as a function of imaginary chemical potential [50]. This leads to the ansatz:

$$F(T, \mu_B) = \frac{p_0 + p_1 x + \dots + p_m x^m}{1 + q_1 x + \dots + q_n x^n}. \quad (11)$$

Ansätze of this form will be considered in this paper for the first time in the literature. We, however, will not consider ansätze of the form of Eq. (9), since by not respecting Roberge-Weiss symmetry, they are unreliable for $|\mu_B/T| > \pi$ (at least in some directions in the complex μ_B plane). Specifically, we will use $m = 1$ and $n = 2$. This specific choice is motivated by three observations. First, the $n = 2$ is the lowest order in the denominator that allows for an arbitrary position of the Lee-Yang zeros in the strip of the complex plane with $-\pi < \text{Im} \mu_B \leq \pi$ (the strip is then periodically repeated). Second, increasing the number of parameters, e.g. taking $n = 3$, we

observed an overfitting of the data, and a corresponding instability in the Lee-Yang zero positions. Third, using fewer parameters (so $m = 0$ instead of $m = 1$) did not allow us to fit all the data with good enough χ^2 values. To have a systematic error estimate on the Lee-Yang zero extraction from the Padé approximants, we will consider, however, different choices for the observable F .

We show the resulting rational function in Fig. 5 in the range where we have data points ($[\pi, 0]$ in imaginary μ_B/T). We picked the example of $T = 140$ MeV with the $\Delta\hat{p}$ ansatz and selected χ_2 and χ_4 as observables. The fit includes χ_1, \dots, χ_4 at 8 imaginary valued chemical potentials, and χ_2, \dots, χ_{10} at $\mu_B = 0$. The shown example has a reduced chi square $\chi^2/\text{ndof} = 45.5/30$.

Note that if one has further information about the analytic structure of the free energy, it is possible to use holomorphic maps to take advantage of this information. In particular Ref. [25] used a method that moves the cut formed from the accumulation of Lee-Yang zeros in the thermodynamic limit (the Lee-Yang edge) to the unit circle. When Ref. [25] applied this approach to the then available lattice data, it found that it made only a small difference compared to the naive Padé approximation approach of Eq. (9) in the final results. We will see that other effects lead to a larger systematic error in the Lee-Yang zero positions, and thus we will not apply this approach in our study. In addition to this basic observation, one should also note that Ref. [25] assumes that cuts starting at the Lee-Yang edge are the only non-analyticities in the free energy. However, in full QCD, this is not correct, as the Roberge-Weiss periodicity means that such discontinuities are repeated an infinite number of times in the imaginary chemical potential direction. How these affect the singularity structure after applying such a holomorphic map has not yet been worked out and should be the subject of future theoretical research.

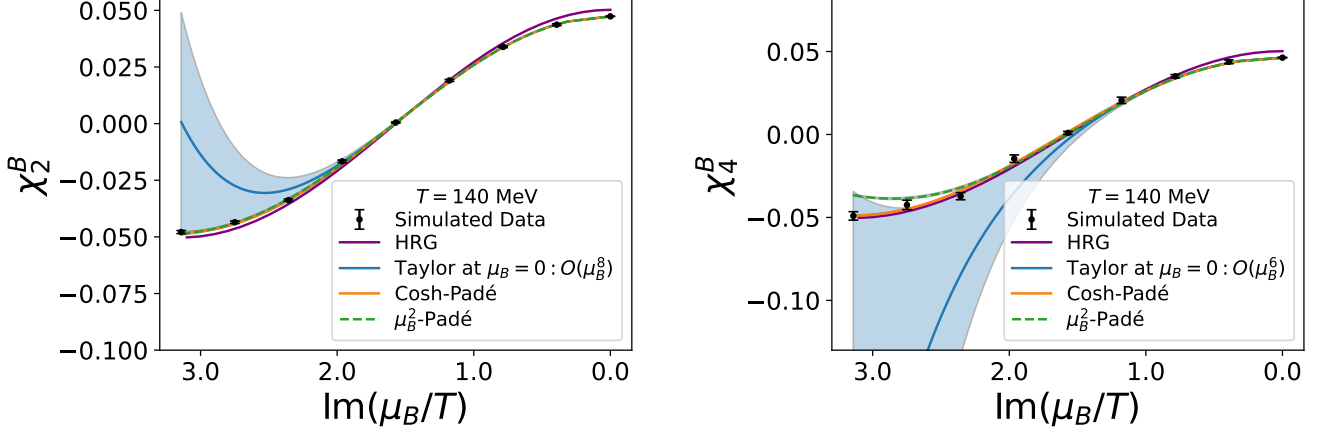


FIG. 5. The result of the fitting of the model in Eq. (11) with $m = 1$ and $n = 2$, using $x = \cosh(\mu_B/T)$ (orange) or $x = \mu_B^2$ (green). The less sophisticated ansatz with $x = \mu_B^2$ offers a poor fit quality, whereas the periodic one is always acceptable. This example shows the fit at $T = 140$ MeV with the $\Delta\hat{p}$ ansatz. Different temperatures are fitted independently.

C. The hadron resonance gas baseline

A common non-critical baseline for the critical end-point search in QCD phenomenology is the hadron resonance gas (HRG) model. In terms of the Taylor coefficients, it satisfies:

$$\chi_2 = \chi_4 = \chi_6 = \chi_8 = \dots \quad (12)$$

Strictly speaking this relation is true in the Boltzmann approximation only, which however is well justified for baryons. While the leading χ_2 coefficient as a function of temperature depends on the actual baryon spectrum, the prediction of Eq. (12) is independent of the exact hadron spectrum used in the construction of the model. Thus, at a finite lattice spacing (where the hadron spectrum is distorted by cut-off effects) Eq. (12) still remains true. This also holds in a finite volume, such as those in our simulations.

The HRG features no critical endpoint. Indeed, by applying the ansatz of Eq. (11) one should get $q_1 = \dots = q_n = 0$, since the pressure in the HRG is simply $p = p_0(T) + p_1(T) \cosh(\mu_B/T)$. By including noise, non-zero coefficients will appear in the denominator. However, in general the position of the zeros of the denominator will not be stable under variations in the noise itself.

In fact, the zeros of the denominator:

$$1 + q_1(\cosh(\hat{\mu}_B) - 1) + q_2(\cosh(\hat{\mu}_B) - 1)^2 \quad (13)$$

are bound to be either close to $\text{Im } \mu_B = \pi/2$ or close to $\text{Im } \mu_B = \pi$, depending on the particular realization of the noise. This is because the imaginary part of the solution to Eq. (13) changes abruptly from π to around $\pi/2$ as the sign of the q_2 coefficient changes, as discussed in more detail in Appendix B. This leads to an instability in the noisy HRG model, where a Lee-Yang zero with either $\text{Im } \mu_B \approx \pi$ or $\text{Im } \mu_B \approx \pi/2$ can appear.

This expectation is confirmed by a mock data analysis, where we used noise with the same relative errors and correlations as our lattice data in addition to the HRG prediction for the Taylor coefficients, and performed the same analysis we employed with the actual lattice data. When we show noisy HRG baselines in this paper, we always show both branches of this instability.

A lattice result consistent with such a noisy HRG baseline does not rule out a CEP. However, it may indicate that we have reached the limits of the applicability of our ansatz. Baryon interactions are encoded in the higher orders ($k \geq 2$) of the fugacity expansion $p/T^4 = \sum_k c_k \cosh(k\hat{\mu}_B)$. We know that c_2, c_3, \dots are suppressed by Boltzmann factors related to two-, three-baryon states, respectively, at low T [47–49]. No matter how small the sub-leading corrections are, they appear in the higher order baryon number fluctuation χ_{2n} enhanced by a factor k^{2n} , and will give a dominant contribution for a high enough order of the Taylor coefficients. Thus, by taking a sufficiently large number of derivatives, one always expects deviations from the HRG model. By not observing such deviations, we see that either the order of our Taylor expansion is not high enough or the statistics is not sufficient (thus, the uncertainties are not small enough) to resolve deviations from the HRG model and thus to constrain the analytic structure of QCD at the given temperature. Thus, we will always compare our Padé approximant's poles with the HRG baseline. Whenever we find agreement, we will exclude those low temperatures from our fit range for the scaling ansatz in Eq. (8). For our dataset, this means that we will have to restrict our fits of the scaling ansatz to temperatures above 130 MeV. Another reason to exclude these data points from further analysis is that they share the same instability in the imaginary part of the Lee-Yang zeros, which fluctuates between π and approximately $\pi/2$.

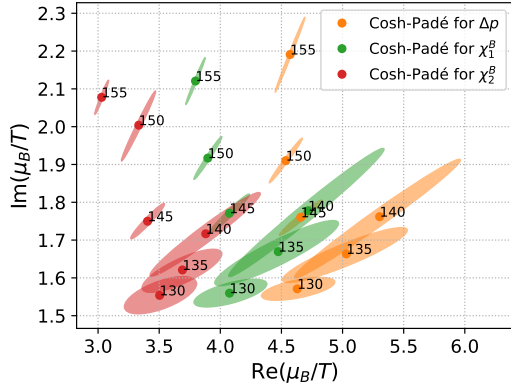


FIG. 6. The extracted Lee-Yang zeros positions for various temperatures in the complex μ_B/T plane. The ellipses represent statistical errors. The different colors represent the choices $F = \Delta p$ (orange), $F = \chi_1^B$ (green) and $F = \chi_2^B$ (red) respectively. The temperatures (in MeV) are indicated next to the particular error ellipse.

D. Systematics of the Lee-Yang zero extraction

One has to remember that even before the scaling ansatz in Eq. (8) is used, each data point on the position of the leading Lee-Yang zero at the different fixed values of the temperature is based on an analytic continuation to complex chemical potentials. Such an analytic continuation could have significant systematic errors. To estimate these, we use three different ansätze for the free energy, distinguished by a different choice of F in Eq. (11). We choose either $\Delta\hat{p}(T, \hat{\mu}_B) = \hat{p}(T, \hat{\mu}_B) - \hat{p}(T, 0)$, χ_1^B or χ_2^B , where $\hat{p} = p/T^4$. The impact of these three different choices is illustrated in Fig. 6, where the estimated Lee-Yang zero positions are shown for different temperatures with the three different choices. A conclusion one can draw from this figure is that, while the imaginary part of the Lee-Yang zeros is stable for different choices of F , the real part is not.

E. Systematics of the extrapolation to the CEP

Supposing that the CEP exists, universality arguments give information about the asymptotic behavior of thermodynamic functions in the vicinity of the critical endpoint. The asymptotic behavior should be of the form given by Eq. (8). However, at the moment we only have data far away from the critical endpoint, where the Lee-Yang zeros are still far from the real axis. We have to perform an extrapolation to a rather distant temperature, to get an estimate of the critical endpoint. To estimate the systematic errors of such a bold extrapolation, we performed fits using four different ansätze. All of which have the same asymptotic behavior, but differ away from the

critical endpoint:

$$\begin{aligned} T - T_{CEP} &\approx A (\text{Im } \mu_{LY})^{\frac{1}{\beta\delta}}, \\ T - T_{CEP} &\approx B (\text{Im } \mu_{LY}^2)^{\frac{1}{\beta\delta}}, \\ T - T_{CEP} &\approx C (\text{Im } \mu_{LY}^3)^{\frac{1}{\beta\delta}}, \\ T - T_{CEP} &\approx D (\text{Im } \mu_{LY}^4)^{\frac{1}{\beta\delta}}. \end{aligned} \quad (14)$$

In the vicinity of the CEP we have

$$\begin{aligned} \text{Im } \mu_{LY}^2 &\sim 2\mu_{CEP} \text{Im } \mu_{LY}, \\ \text{Im } \mu_{LY}^3 &\sim 3\mu_{CEP}^2 \text{Im } \mu_{LY} - (\text{Im } \mu_{LY})^3, \\ \text{Im } \mu_{LY}^4 &\sim 4\mu_{CEP}^3 \text{Im } \mu_{LY} - 4\mu_{CEP} (\text{Im } \mu_{LY})^3. \end{aligned}$$

Since all of these functions have the same asymptotic behavior near the critical endpoint, there is no reason to prefer one of these ansätze to the others. In Fig. 7 we show these four different fits on the same data, together with the noisy HRG baseline for comparison. Below $T = 130$ MeV we find that the lattice results are consistent with the baseline. As explained previously, this means that the data quality in this range of temperatures is not sufficient to constrain the analytic structure of the QCD free energy. Thus, those temperatures (shown in grey in Fig. 7) are left out from our fits. With this temperature range restriction, one can see that depending on the choice of the scaling variable, one can get a CEP prediction compatible with the nuclear liquid-gas transition, and just as well one compatible with a high-temperature chiral critical endpoint.

Similarly important is the choice of the temperature range of the fit. This is illustrated in Fig. 8., where one can see that the systematic error due to the choice of the temperature range is also rather large.

Let us also underline an important difference between extrapolations based on Eq. (8) and other extrapolations in lattice field theory, such as a continuum limit extrapolation. In our case each point (each temperature) used for the extrapolation is itself the result of an extrapolation in the complex chemical potential plane. The lower the temperature, the more relevant the data point is, due to its closer proximity to the critical end point. Thus, although data at lower temperatures more reliably guide the extrapolation toward a Lee-Yang zero on the real μ_B axis, they require much higher statistics to combat the still unresolved sign problem. This is because the higher orders in the extrapolation scheme are the ones that will be most sensitive to baryon interactions, but also the most difficult ones to determine. In short, unfortunately, the reliability of the data diminishes with decreasing temperature. This is in contrast with the continuum extrapolation, where at smaller lattice spacing the simulations are only more expensive, but systematic errors do not rise. While fine lattices are always included in the continuum extrapolations, in our systematic analysis we will also consider extrapolations where some of the lowest temperatures (closer to a CEP) are discarded.

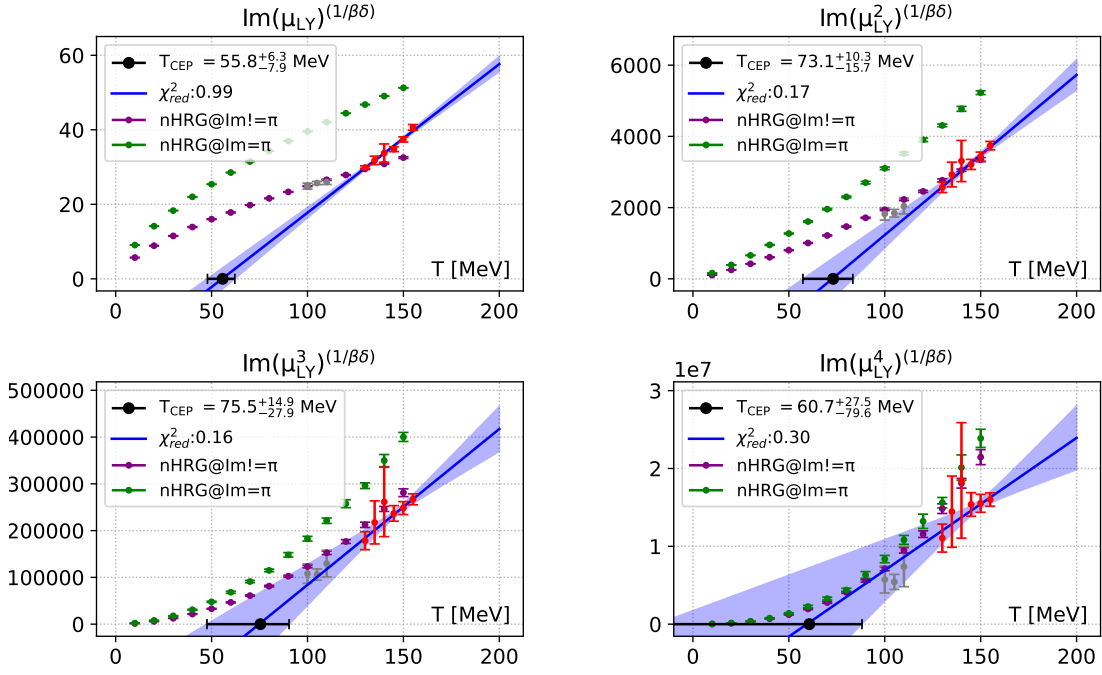


FIG. 7. Extrapolation of the critical temperature using the four different ansätze in Eq. (14). Near the CEP, all four ansätze are asymptotically equivalent, though farther away they lead to different behavior. All four fits have good χ^2 values, but they lead to different values for the critical temperature. The two (unstable) branches of the noisy HRG model (nHRG) baseline is also shown.

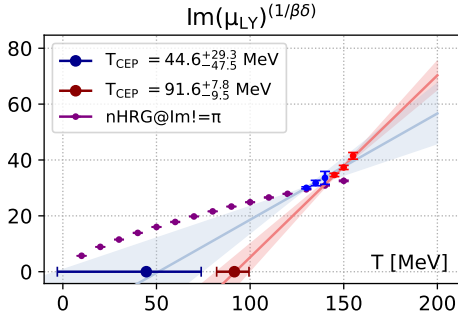


FIG. 8. Extrapolation of T_{CEP} using two different temperature ranges.

F. Weighting and posterior distribution for T_{CEP}

In our final results we will consider the following choices to estimate systematic errors:

1. The different choices for the analytic continuation to complex chemical potentials, corresponding to $F = \Delta p$, χ_1^B or χ_2^B respectively in Eq. (11) (3 choices).
2. Four different choices of the scaling ansatz to extrapolate the position of the critical endpoint, shown in Eq. (14).
3. Six different choices for the temperature range in

the extrapolations in Eq. (14). The choices are:

$$\begin{aligned} & [130\text{MeV}, 145\text{MeV}], [135\text{MeV}, 150\text{MeV}], \\ & [140\text{MeV}, 155\text{MeV}], [130\text{MeV}, 150\text{MeV}], \\ & [135\text{MeV}, 155\text{MeV}], [130\text{MeV}, 155\text{MeV}]. \end{aligned}$$

These lead to a total of $3 \times 4 \times 6 = 72$ different analyses. All of the fits have acceptable χ^2 values, thus we combine them with uniform weights. The different analyses are combined into a single distribution function for T_{CEP} by assuming Gaussian distributions for the individual fits. Combining the different fits into a single cumulative distribution function, we then proceed using the following formula:

$$CDF(T_{CEP}) = \sum_j w_j \frac{1}{2} \left(1 - \text{erf} \left(\frac{m_j - T_{CEP}}{\sqrt{2}\sigma_j} \right) \right), \quad (15)$$

where m_j and σ_j are the mean and the statistical error of the given analysis. Since we use uniform weights, we take $w_j = 1/72$ for all fits.

Taking the results at face value, we arrive at an upper bound on the location of the chiral critical endpoint position. With 84% probability, the critical endpoint is either below $T = 103$ MeV or it does not exist. Assuming that the CEP exists, its most likely position (the peak of the posterior distribution for T_{CEP}) is in the temperature bin near 70 MeV.

The probability distribution for T_{CEP} has a non-negligible part in the very low temperature range. This

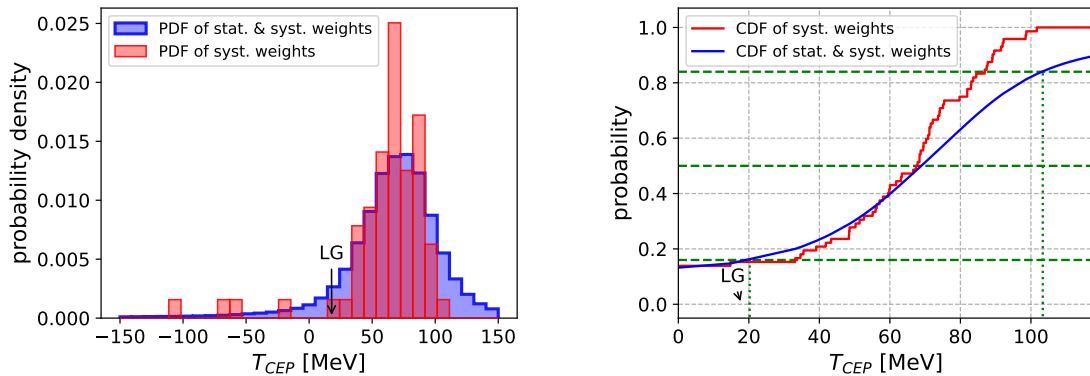


FIG. 9. The histogram (left) and the cumulative distribution function for the critical endpoint temperature T_{CEP} . (We indicate the location of the liquid-gas critical endpoint with the label LG [51]).

means that the data is consistent with the non-existence of chiral critical endpoint, while the Lee-Yang zeros getting closer to the real axis being a consequence of the existence of the nuclear liquid-gas critical endpoint. Such a scenario was presented e.g. in Ref. [52], where in a van der Waals type generalization of the hadron resonance gas model, echoes of the nuclear liquid-gas critical endpoint could be observed at surprisingly large temperatures.

IV. SUMMARY AND DISCUSSION

We have performed large statistics lattice simulations using 4HEX improved staggered fermions on $16^3 \times 8$ lattices at zero and purely imaginary baryochemical potentials. On these ensembles, we calculated Taylor coefficients of the pressure up to tenth order at zero, and up to the fourth order at imaginary chemical potentials. We used this data to construct rational function approximations of the QCD free energy, and to approximate the position of the Lee-Yang zero closest to the origin in the complex chemical potential plane. The imaginary part of the Lee-Yang zeros was then extrapolated to zero value, in order to estimate the temperature of the critical endpoint of QCD.

The main result of our manuscript is an upper bound on the location of the critical endpoint position. With 84% probability, the critical endpoint is either below $T = 103$ MeV or it does not exist. Assuming that the CEP exists, its most likely position is near 70 MeV.

Our results are compatible with the estimates of the CEP position from functional methods [10, 11], but are in slight tension with recent lattice estimates [25, 26]. Note that neither these, nor our results have been continuum extrapolated, and the lattice artefacts are not expected to be the same.

Our work has some important technical caveats:

1. The continuum limit was not performed, as only

$N_\tau = 8$ lattices were used.

2. The thermodynamic limit was not taken, nor a finite volume scaling analysis was performed.
3. Because of a finite order truncation of the Taylor expansions, the Lee-Yang zero extractions at fixed temperature suffer from systematic errors.
4. The extrapolation of the critical temperature T_{CEP} also suffers from systematic errors, since the Lee-Yang zero positions have to be extrapolated to a region of the phase diagram that is quite far away from where the lattice data is available.

In principle it is possible to alleviate all four of these problems, but for the moment they lead to a rather large uncertainty in the position of the CEP.

Caveats 1 and 2 cannot be addressed with the dataset used for this work. While in our recent publication [6] we observed quite mild cut-off effects for this discretization for Taylor coefficients up to sixth order, this does not automatically guarantee similarly small cut-off effects for the 8th and 10th order coefficients calculated in this work. Similarly, for temperatures below the crossover, our earlier comparison between the continuum extrapolated data [6] at a smaller volume $LT = 2$ and our $N_t = 12$ 4stout improved data at a larger volume ($LT = 4$) were compatible within errors, indicating mild finite volume effects. However, this does not guarantee that the same would hold for the larger 8th and 10th order coefficients calculated in this work. Ultimately one has to perform a similar analysis for at least two larger volumes and at least two smaller lattice spacings. In view of Fig. 1, this will be a serious challenge, since the costs of the eighth order coefficient scales with the sixth power of the volume.

On the other hand, caveats 3 and 4 are considered in our final systematic errors, and lead to the facts that our analysis does not provide a sharp prediction for the CEP position, but only a bound. Previous works in

Refs. [25, 26] have not taken all of these systematic effects into account. This is the reason why we obtain significantly larger final errors, even though our input data are much more precise. Caveat 3 is the main reason why only the temperature of the critical endpoint can be estimated, but not its chemical potential. The real part of the position of the Lee-Yang zeros is much less stable under a change of the ansatz used for the analytic continuation compared to the imaginary part.

In principle, it is also possible to extract Lee-Yang zeros without relying on Taylor coefficients, and thus without any truncation errors, using the canonical formalism as was done in Ref. [23] for $N_\tau = 4$ lattices. This method has a good chance to significantly reduce or even completely remove issue 3. How the signal-to-noise ratios of this method change at finer lattices, however, remains to be seen.

Extending the temperature range of the available lattice simulations should help with caveat 4. However, this is not a trivial task, as the signal to noise ratio of the Taylor coefficients also deteriorates at smaller temperatures. In addition, corrections to the hadron resonance gas model (the subleading fugacity expansion coefficients) become smaller at low temperatures, making the contributions responsible for criticality harder to access. Thus, extending datasets to lower temperatures might require new algorithmic ideas. Of course, as the quality of the data increases and deviations from the hadron resonance gas can be resolved at lower temperatures, one must also increase the number of free parameters in the ansatz used to extract the Lee-Yang zeros.

A. Acknowledgements

This work is supported by the MKW NRW under the funding code NW21-024-A. Further funding was received from the DFG under the Project No. 496127839. This work was also supported by the Hungarian National Research, Development and Innovation Office, NKFIH Grant No. KKP126769. This work was also supported by the NKFIH excellence grant TKP2021_NKTA_64. This work is also supported by the Hungarian National Research, Development and Innovation Office under Project No. FK 147164. This material is also based upon work supported by the National Science Foundation under grants No. PHY-2208724, and PHY-2116686, and within the framework of the MUSES collaboration, under grant number No. OAC- 2103680. This material is also based upon work supported by the U.S. Department of Energy, Office of Science, Office of Nuclear Physics, under Award Numbers DE-SC0022023 and DE-SC0025025, as well as by the National Aeronautics and Space Agency (NASA) under Award Number 80NSSC24K0767. The authors gratefully acknowledge the Gauss Centre for Supercomputing e.V. (www.gauss-centre.eu) for funding this project by providing computing time on the GCS Supercomputer HAWK at HLRS, Stuttgart. An award of

computer time was provided by the INCITE program. This research used resources of the Argonne Leadership Computing Facility, which is a DOE Office of Science User Facility supported under Contract DE-AC02-06CH11357.

Appendix A: Zeros of χ_2^B and χ_4^B at purely imaginary baryochemical potential

The simplest way to understand why both χ_2^B and χ_4^B have a zero at purely imaginary chemical potential at temperatures below the crossover is to first start with the hadron resonance gas model (in the Boltzmann approximation), where the pressure is approximated to be:

$$p(T, \mu_B) \approx p_0(T) + p_1(T) \cosh\left(\frac{\mu_B}{T}\right). \quad (\text{A1})$$

Differentiating with respect to μ_B/T and writing $\mu_B = i\mu_I$ we get a zero for both χ_2^B and χ_4^B at $\mu_I/T = \pi/2$. This zero is a property of a free gas of hadrons. The ratio χ_4^B/χ_2^B is equal to 1 in this model. Near $\mu_I = \pi/2$ this value of 1 is realized as a 0/0 limit. However, the HRG model is not exact. A more accurate approximation is given by the next order of the fugacity expansion [47–49]:

$$p(T, \mu_B) \approx p_0(T) + p_1(T) \cosh\left(\frac{\mu_B}{T}\right) + p_2(T) \cosh\left(2\frac{\mu_B}{T}\right), \quad (\text{A2})$$

where $p_2(T) \ll p_1(T)$. Now differentiating with respect to μ_B/T and writing $\mu_B = i\mu_I$ we arrive at the conclusion that both χ_2^B and χ_4^B have a zero in the vicinity of $\mu_I/T = \pi/2$, however, the exact positions of the zeros do not coincide. Using a leading order Taylor expansion near $\mu_I/T = \pi/2$ we get the zero for χ_2^B at the position $\mu_I \approx \frac{\pi}{2} - 4p_2(T)/p_1(T)$ while the zero for χ_4^B to be at the position $\mu_I \approx \frac{\pi}{2} - 16p_2(T)/p_1(T)$. This leads to a divergence in χ_4^B/χ_2^B at $\mu_I \approx \frac{\pi}{2} - 4p_2(T)/p_1(T)$. This divergence is physical, but it is a property of a weakly interacting gas of hadrons and has nothing to do with criticality. Thus, while it limits the convergence of the Taylor expansion of χ_4^B/χ_2^B , this is only an inconvenience when one tries to look for the critical endpoint. Note, however, that this divergence in χ_4^B/χ_2^B at imaginary μ_B does not limit the radius of convergence of the Taylor expansions of χ_2^B and χ_4^B themselves and thus taking the ratio of the Taylor coefficients, instead of the Taylor expansion of the ratio is more reasonable.

Appendix B: Behavior of the denominator

The denominator for the Padé approximants used in our study reads

$$1 + q_1(\cosh \hat{\mu}_B - 1) + q_2(\cosh \hat{\mu}_B - 1)^2.$$

The estimated Lee-Yang zeros are given by the zeros of this denominator. The imaginary part of these zeros

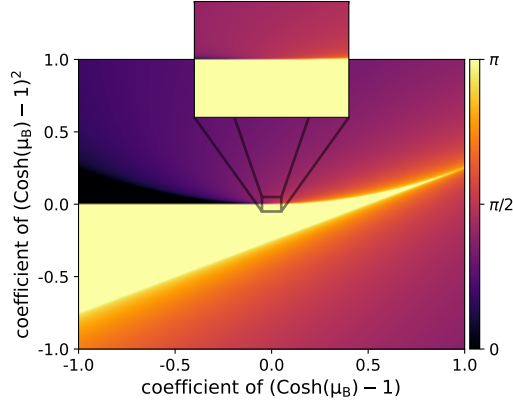


FIG. 10. Imaginary part of the zeros of the denominator for the Roberge-Weiss symmetric Padé approximant used in our study as a function of the q_1 and q_2 coefficients. A zoomed in version near the origin is also shown on top.

is then used for the extrapolation to the critical point. Since the ansatz respects Roberge-Weiss symmetry, the imaginary part of the Lee-Yang zeros is restricted to be between zero and π , after which the function periodically repeats itself. The imaginary part as a function of the coefficients q_1 and q_2 is shown in Fig. 10. One can see that the function actually takes all values between zero and π and thus is in principle able to resolve Lee-Yang zeros close to the origin. A zoom in version near the origin is also shown on top. Here, we see the instability between the π and approximately $\pi/2$ values mentioned in the main text, depending on the sign of the coefficient multiplying $(\cosh(\hat{\mu}_B) - 1)^2$.

Appendix C: Statistics

T [MeV]	β	m_l	m_s	# configurations at $\mu_B = i\pi(j/8)$									
	$16^3 \times 8$ lattice			$j = 0$	$j = 1$	$j = 2$	$j = 3$	$j = 4$	$j = 5$	$j = 6$	$j = 7$	$j = 8$	
100	0.4846	0.00490631	0.1355610	915010	-	-	-	-	-	-	-	-	-
105	0.5050	0.00458740	0.1267500	894220	-	-	-	-	-	-	-	-	-
110	0.5236	0.00432111	0.1193920	760795	-	-	-	-	-	-	-	-	-
115	0.5406	0.00409845	0.1132400	1054502	-	-	-	-	-	-	-	-	-
120	0.5560	0.00390982	0.1080280	1082567	-	-	-	-	-	-	-	-	-
125	0.5700	0.00374705	0.1035310	1726868	-	-	-	-	-	-	-	-	-
130	0.5829	0.00360381	0.0995733	2132329	-	96440	-	96082	-	95775	-	95625	-
135	0.5947	0.00347548	0.0960274	1453169	110859	105287	104348	120205	103744	103749	103196	103084	-
140	0.6056	0.00335869	0.0928007	4010320	99904	105232	104911	359058	103501	99483	102589	113865	-
145	0.6158	0.00325107	0.0898270	2579944	106703	106386	105027	121944	103958	103239	102471	115049	-
150	0.6252	0.00315088	0.0870590	1688860	114258	114018	112067	117290	109804	97932	96239	109087	-
155	0.6341	0.00305689	0.0844619	1623503	109132	108649	107158	125765	104061	102762	101464	115855	-
160	0.6425	0.00296817	0.0820105	2229437	112026	111086	108615	128345	104466	95570	101203	108589	-
165	0.6504	0.00288403	0.0796857	1768242	103692	101652	89855	121047	95726	92934	86765	105389	-
170	0.6579	0.00280394	0.0774727	1204210					-				
175	0.6651	0.00272748	0.0753604	1602383					-				
180	0.6719	0.00265434	0.0733394	1357330					-				
185	0.6785	0.00258424	0.0714026	855048					-				
190	0.6848	0.00251696	0.0695436	318710					-				
195	0.6909	0.00245231	0.0677573	362672					-				
200	0.6968	0.00239013	0.0660393	324768					-				
205	0.7025	0.00233028	0.0643856	159500					-				
210	0.7080	0.00227263	0.0627928	260084					-				
220	0.7188	0.00216352	0.0597782	249068					-				
230	0.7290	0.00206205	0.0569745	257480					-				
240	0.7389	0.00196759	0.0543644	270856					-				
250	0.7485	0.00187961	0.0519336	430495					-				
260	0.7580	0.00179768	0.0496700	281616					-				
280	0.7765	0.00165052	0.0456040	289961					-				
300	0.7946	0.00152351	0.0420946	297512					-				

TABLE I. Simulation parameters and statistics of the used ensembles. The configurations were separated by 20 RHMC updates. On each configuration a full eigenvalue analysis has been carried out at both the light and strange masses.

-
- [1] Y. Aoki, G. Endrodi, Z. Fodor, S. Katz, and K. Szabo, *Nature* **443**, 675 (2006), arXiv:hep-lat/0611014 [hep-lat].
- [2] C. Bonati, M. D’Elia, F. Negro, F. Sanfilippo, and K. Zambello, *Phys. Rev. D* **D98**, 054510 (2018), arXiv:1805.02960 [hep-lat].
- [3] A. Bazavov *et al.* (HotQCD), *Phys. Lett. B* **795**, 15 (2019), arXiv:1812.08235 [hep-lat].
- [4] S. Borsanyi, Z. Fodor, J. N. Guenther, R. Kara, S. D. Katz, P. Parotto, A. Pasztor, C. Ratti, and K. K. Szabo, *Phys. Rev. Lett.* **125**, 052001 (2020), arXiv:2002.02821 [hep-lat].
- [5] D. Bollweg, J. Goswami, O. Kaczmarek, F. Karsch, S. Mukherjee, P. Petreczky, C. Schmidt, and P. Scior (HotQCD), *Phys. Rev. D* **105**, 074511 (2022), arXiv:2202.09184 [hep-lat].
- [6] S. Borsanyi, Z. Fodor, J. N. Guenther, S. D. Katz, P. Parotto, A. Pasztor, D. Pesznyak, K. K. Szabo, and C. H. Wong, *Phys. Rev. D* **110**, L011501 (2024), arXiv:2312.07528 [hep-lat].
- [7] S. Borsanyi, Z. Fodor, J. N. Guenther, S. K. Katz, K. K. Szabo, A. Pasztor, I. Portillo, and C. Ratti, *JHEP* **10**, 205 (2018), arXiv:1805.04445 [hep-lat].
- [8] P. Kovács, Z. Szép, and G. Wolf, *Phys. Rev. D* **93**, 114014 (2016), arXiv:1601.05291 [hep-ph].
- [9] W.-j. Fu, X. Luo, J. M. Pawłowski, F. Rennecke, and S. Yin, *Phys. Rev. D* **111**, L031502 (2025), arXiv:2308.15508 [hep-ph].
- [10] P. Isserstedt, M. Buballa, C. S. Fischer, and P. J. Gunkel, *Phys. Rev. D* **100**, 074011 (2019), arXiv:1906.11644 [hep-ph].
- [11] F. Gao and J. M. Pawłowski, *Phys. Rev. D* **102**, 034027 (2020), arXiv:2002.07500 [hep-ph].
- [12] M. Hippert, J. Grefa, T. A. Manning, J. Noronha, J. Noronha-Hostler, I. Portillo Vazquez, C. Ratti, R. Rougemont, and M. Trujillo, *Phys. Rev. D* **110**, 094006 (2024), arXiv:2309.00579 [nucl-th].
- [13] S. Borsányi, Z. Fodor, J. N. Guenther, R. Kara, S. D. Katz, P. Parotto, A. Pásztor, C. Ratti, and K. K. Szabó, *Phys. Rev. Lett.* **126**, 232001 (2021), arXiv:2102.06660 [hep-lat].
- [14] S. Borsanyi, Z. Fodor, J. N. Guenther, R. Kara, P. Parotto, A. Pasztor, C. Ratti, and K. K. Szabo, *Phys. Rev. D* **105**, 114504 (2022), arXiv:2202.05574 [hep-lat].
- [15] M. Kahangirwe, I. Gonzalez, J. A. Muñoz, C. Ratti, and V. Vovchenko, (2024), arXiv:2408.04588 [nucl-th].
- [16] R. Wen, S. Yin, and W.-j. Fu, *Phys. Rev. D* **110**, 016008 (2024), arXiv:2403.06770 [hep-ph].
- [17] A. Abuali, S. Borsányi, Z. Fodor, J. Jahan, M. Kahangirwe, P. Parotto, A. Pásztor, C. Ratti, H. Shah, and S. A. Trabulsi, (2025), arXiv:2504.01881 [hep-lat].
- [18] H. Shah, M. Hippert, J. Noronha, C. Ratti, and V. Vovchenko, (2024), arXiv:2410.16206 [hep-ph].
- [19] S. Borsanyi, Z. Fodor, J. N. Guenther, P. Parotto, A. Pasztor, C. Ratti, V. Vovchenko, and C. H. Wong, (2025), arXiv:2502.10267 [hep-lat].
- [20] M. Marczenko, M. Szymański, and G. Kovács, (2025), arXiv:2504.04446 [hep-ph].
- [21] Z. Fodor and S. Katz, *JHEP* **0404**, 050 (2004), arXiv:hep-lat/0402006 [hep-lat].
- [22] M. Giordano and A. Psztor, *Phys. Rev. D* **D99**, 114510 (2019), arXiv:1904.01974 [hep-lat].
- [23] M. Giordano, K. Kapas, S. D. Katz, D. Nogradi, and A. Pasztor, *Phys. Rev. D* **101**, 074511 (2020), arXiv:1911.00043 [hep-lat].
- [24] P. Dimopoulos, L. Dini, F. Di Renzo, J. Goswami, G. Nicotra, C. Schmidt, S. Singh, K. Zambello, and F. Ziesché, *Phys. Rev. D* **105**, 034513 (2022), arXiv:2110.15933 [hep-lat].
- [25] G. Basar, *Phys. Rev. C* **110**, 015203 (2024), arXiv:2312.06952 [hep-th].
- [26] D. A. Clarke, P. Dimopoulos, F. Di Renzo, J. Goswami, C. Schmidt, S. Singh, and K. Zambello, (2024), arXiv:2405.10196 [hep-lat].
- [27] V. V. Skokov, *SciPost Phys. Lect. Notes* **91**, 1 (2025), arXiv:2411.02663 [hep-ph].
- [28] S. Borsányi, Z. Fodor, J. N. Guenther, R. Kara, P. Parotto, A. Pásztor, L. Pirelli, and C. H. Wong, *Phys. Rev. D* **111**, 014506 (2025).
- [29] Z. Fodor and S. Katz, *Phys. Lett. B* **B534**, 87 (2002), arXiv:hep-lat/0104001 [hep-lat].
- [30] Z. Fodor and S. Katz, *JHEP* **0203**, 014 (2002), arXiv:hep-lat/0106002 [hep-lat].
- [31] S. Borsanyi, Z. Fodor, M. Giordano, J. N. Guenther, S. D. Katz, A. Pasztor, and C. H. Wong, *Phys. Rev. D* **107**, L091503 (2023), arXiv:2208.05398 [hep-lat].
- [32] S. Borsanyi, Z. Fodor, M. Giordano, J. N. Guenther, S. D. Katz, A. Pasztor, and C. H. Wong, *Phys. Rev. D* **109**, 054509 (2024), arXiv:2308.06105 [hep-lat].
- [33] S. Borsanyi, Z. Fodor, J. N. Guenther, P. Parotto, A. Pasztor, L. Pirelli, K. K. Szabo, and C. H. Wong, *Phys. Rev. D* **110**, 114507 (2024), arXiv:2410.06216 [hep-lat].
- [34] A. Hasenfratz and D. Toussaint, *Nucl. Phys.* **B371**, 539 (1992).
- [35] C. Allton, M. Doring, S. Ejiri, S. Hands, O. Kaczmarek, *et al.*, *Phys. Rev. D* **D71**, 054508 (2005), arXiv:hep-lat/0501030 [hep-lat].
- [36] We supply these coefficients as ancillary files along with the submission.
- [37] M. Stephanov, *Phys. Rev. Lett.* **107**, 052301 (2011), arXiv:1104.1627 [hep-ph].
- [38] D. Mroczek, A. R. Nava Acuna, J. Noronha-Hostler, P. Parotto, C. Ratti, and M. A. Stephanov, *Phys. Rev. C* **103**, 034901 (2021), arXiv:2008.04022 [nucl-th].
- [39] W.-j. Fu, X. Luo, J. M. Pawłowski, F. Rennecke, R. Wen, and S. Yin, *Phys. Rev. D* **104**, 094047 (2021), arXiv:2101.06035 [hep-ph].
- [40] A. Andronic, P. Braun-Munzinger, and J. Stachel, *Nucl. Phys.* **A772**, 167 (2006), arXiv:nucl-th/0511071 [nucl-th].
- [41] F. Becattini, M. Bleicher, T. Kollegger, T. Schuster, J. Steinheimer, *et al.*, *Phys. Rev. Lett.* **111**, 082302 (2013), arXiv:1212.2431 [nucl-th].
- [42] P. Alba, W. Alberico, R. Bellwied, M. Bluhm, V. Mantovani Sarti, *et al.*, *Phys. Lett. B* **B738**, 305 (2014), arXiv:1403.4903 [hep-ph].
- [43] V. Vovchenko, V. V. Begun, and M. I. Gorenstein, *Phys. Rev. C* **C93**, 064906 (2016), arXiv:1512.08025 [nucl-th].
- [44] C. Itzykson, R. B. Pearson, and J. B. Zuber, *Nucl. Phys. B* **220**, 415 (1983).
- [45] P. Butera and M. Pernici, *Phys. Rev. E* **86**, 011104 (2012), arXiv:1206.0872 [cond-mat.stat-mech].

- [46] F. Gliozzi, Phys. Rev. Lett. **111**, 161602 (2013), arXiv:1307.3111 [hep-th].
- [47] V. Vovchenko, A. Pasztor, Z. Fodor, S. D. Katz, and H. Stoecker, Phys. Lett. **B775**, 71 (2017), arXiv:1708.02852 [hep-ph].
- [48] P. Huovinen and P. Petreczky, Phys. Lett. **B777**, 125 (2018), arXiv:1708.00879 [hep-ph].
- [49] R. Bellwied, S. Borsanyi, Z. Fodor, J. N. Guenther, S. D. Katz, P. Parotto, A. Pasztor, D. Pesznyak, C. Ratti, and K. K. Szabo, Phys. Rev. D **104**, 094508 (2021), arXiv:2102.06625 [hep-lat].
- [50] A. Roberge and N. Weiss, Nucl.Phys. **B275**, 734 (1986).
- [51] J. B. Elliott, P. T. Lake, L. G. Moretto, and L. Phair, Phys. Rev. C **87**, 054622 (2013).
- [52] V. Vovchenko, M. I. Gorenstein, and H. Stoecker, Phys. Rev. Lett. **118**, 182301 (2017), arXiv:1609.03975 [hep-ph].